

Constraints on Microcontact Printing Imposed by Stamp Deformation

C. Y. Hui*

Department of Theoretical & Applied Mechanics, Cornell University, Ithaca, New York 14853

A. Jagota

The DuPont Company, Experimental Station, Delaware 19880-0356

Y. Y. Lin

Department of Mechanical Engineering, University of New Mexico at Albuquerque, Albuquerque, New Mexico 87110

E. J. Kramer

Department of Materials, University of California, Santa Barbara, California 93106

Received August 27, 2001. In Final Form: November 5, 2001

Stamp deformation can affect the dimensional stability of the microcontact printing process. We consider limitations imposed due to reversible deformation of a single stamp. Detailed analyses of several modes of stamp deformation have been carried out. Stability criteria have been obtained for both vertical and lateral collapse of surface relief features, including buckling. The shape change of surface features imposed by surface tension has been analyzed, and the corresponding internal stresses are given in closed form. The residual stresses induced by chemical and thermal shrinkage when the elastomeric stamp is bonded to a stiff substrate are analyzed. In addition, the relation between applied load and displacement of a stamp supported by a stiff substrate is given in closed form. Contact stresses between the stamp and substrate have been analyzed both analytically and numerically by a finite element method. The role of adhesion in determining the contact area is clarified. The effect of surface roughness on the contact mechanics has been studied, and closed form solutions have been obtained for surface asperities that are periodically distributed. The contact mechanics of stamps with smooth relief features has been studied, and the dependence of contact area on the work of adhesion and the applied pressure is given in closed form. The force required to separate the stamp from the substrate has been estimated using a fracture mechanics approach. The stability and contact mechanics results are summarized by a stability and contact map.

1. Introduction

In microcontact printing (μ CP),^{1–3} ink (typically a chemical reactant) is applied to an elastomeric stamp with a pattern of surface relief. A schematic of the surface relief is shown in Figure 1, where the stamp surface consists of micron size flat punches of width $2a$ and height h . Ideal punches have very sharp corners. Ink is transferred from the stamp to the substrate by bringing the punches into contact with the substrate surface. The stamps are typically fabricated by curing liquid to an elastomer, commonly poly(dimethylsiloxane) (PDMS), on a silicon master fabricated using traditional optical lithography and etching techniques. Sufficiently low adhesion of the elastomer to the master allows the stamps to be peeled from the master. Under ideal conditions, the peeled elastomer stamp is an exact negative replica of the master.

Several advantages of μ CP and related methods over conventional optical lithography have been noted.⁴ For example, they are not subject to diffraction limitations

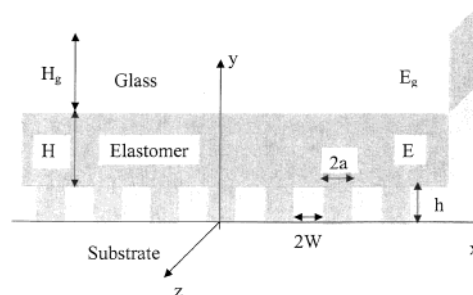


Figure 1. Schematic of a stamp bonded to a glass layer. The punches are identical with width $2a$ and height $h \ll H$. Their length in the z direction is much greater than a and w .

and are relatively simpler and inexpensive. The flexibility of the stamp enables patterning of curved surfaces. Also, the methods are compatible with a wider range of organic and biological materials. There are limitations to μ CP, several of which arise due to stamp deformation. As pointed out by Delamarche et al.,⁵ because of the low modulus of PDMS (typically, the shear modulus of PDMS $G \leq 1$ MPa), only a small subset of the features accessible by microfabrication of patterns in silicon form stable,

* To whom correspondence should be addressed. E-mail: ch45@cornell.edu.

(1) Kumar, A.; Whitesides, G. M. *Appl. Phys. Lett.* **1993**, *63*, 2002.

(2) Kumar, A.; Biebuyck, H. A.; Whitesides, G. M. *Langmuir* **1994**, *10*, 1498.

(3) Biebuyck, H. A.; Larsen, N. B.; Delamarche, E.; Michel, B. *IBM J. Res. Dev.* **1997**, *41* (1), 159.

(4) Mirkin, C. A.; Rogers, J. A. *MRS Bull.* **2001**, *26* (7), 506.

(5) Delamarche, E.; Schmid, H.; Michel, B.; Biebuyck, H. *Adv. Mater.* **1997**, *9*, 741.

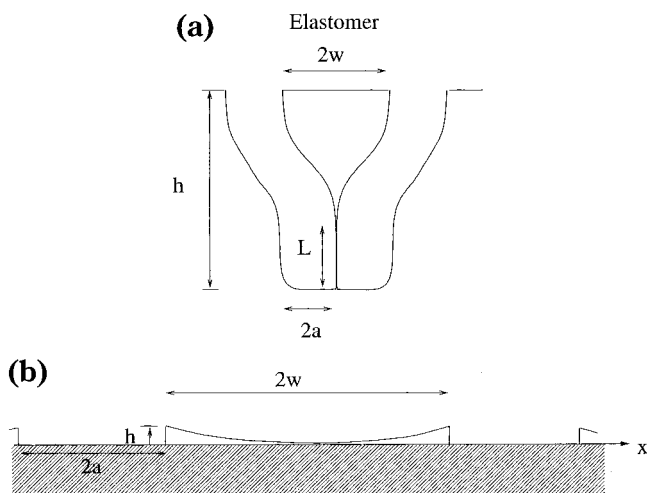


Figure 2. Two neighboring punches adhere to each other by surface forces (a). Contact of the stamp "roof" with the substrate due to an applied compressive load (b)

useful structures on the surface of the stamp. For example, Biebuyck et al.³ have experimentally demonstrated that if the aspect ratio $h/2a$ is too large, the punches can collapse under their own weight (buckling). Also, lateral collapse of neighboring punches can occur during the inking process, where the capillary and other forces experienced by the punches are sufficiently large to cause contact between them. Once contact occurs, punches may adhere to each other due to surface adhesive forces^{5,6} (see Figure 2a). On the other hand, when the aspect ratio is too low, all surfaces of the stamp (not only the raised punches) can be deformed into contact with the substrate as illustrated in Figure 2b. Once contact occurs, the contact area increases due to the action of surface forces near the edge of contact.⁵

A limitation not addressed by Delamarche et al.⁵ is the effect of surface tension on the relief pattern. Due to the low modulus of the elastomer, the relief pattern will not retain its shape after release from the master. For example, consider an idealized silicon master with perfectly sharp corners. After release, surface tension forces will deform the as-molded sharp corners of the punches into smooth equilibrium shapes that can be substantially different from their prerelease forms. This effect is particularly important for high-resolution patterns where the dimensions of individual punches are less than 1 micron.

Often, the stamps are bonded to stiffer layers to improve dimensional stability and handling.⁶⁻⁷ However, the shrinkage of the elastomeric layer cast against the stiff layer gives rise to residual stresses, which can cause small nonuniform distortions, as reported in ref 8.

The easiest way to prevent dimensional instability is to increase the modulus of the elastomer. This approach also has limitations. First, a high-modulus polymer (e.g., a glass) can increase the stress due to the chemical and thermal shrinkage in the curing process, and this can cause the newly formed stamp to separate from the master.⁶ Second, it is considerably more difficult for a high-modulus polymer to establish conformal contact with the substrate in the presence of surface roughness. Third, increasing the modulus often results in a decrease of

fracture toughness. This decrease can seriously affect the resolution and the reliability of the stamp since the highly inhomogeneous stress field underneath the punch increases as the modulus increases. The stress concentration at the sharp corners may lead to plastic deformation (crazes and shear bands in glassy polymers) and cracking of the stamp or the substrate.

Although the limitations mentioned above are well documented qualitatively, the present authors are unaware of detailed analytical models of these problems. In this work, we use contact and fracture mechanics to establish criteria for pattern stability and conformality. We expect that these criteria will provide guidelines for the design of high-resolution stamps. We restrict our attention here to reversible deformation; constraints on the process due to inelastic deformation or fracture (other than interfacial separation) are *not* considered.

The outline of this paper is as follows: in section 2, we state and define the geometry of the problem. In section 3, we establish criteria for stamp stability under applied load. These include buckling, lateral collapse, and surface contact. The first two cases are relevant for high aspect ratio stamps, whereas the surface contact mode is relevant for stamps with low aspect ratios. In section 4, the shape change caused by surface tension after the stamp is released is considered. In section 5, we address the problem of residual stresses generated by thermal and chemical shrinkage when the elastomeric stamp is bonded to a stiffer layer. An exact solution of the internal stresses and deformation is given. In section 6, analytical expressions for the stress field underneath the punches are obtained and the effect of surface forces on the deformation of the punch is considered. In section 7, we consider the effect of surface roughness and estimate the normal pressure required to bring the stamp into intimate contact with the substrate. This result allows us to establish an upper limit for the modulus of the elastomer suitable for μ CP. In section 8, a theory of microcontact printing based on punches with smooth surface relief (nonrectangular) is proposed. The basic idea is to obtain submicron resolution without submicron size relief. In section 9, an estimate is given for the force needed to detach the stamp from a substrate. The results of the previous sections are summarized in section 10 and presented as a stability and contact map.

2. Geometry and Definitions

Most of the results developed in this work are for a periodic array of identical punches, as drawn in Figure 1. The lateral dimension of the stamp, D (not drawn), is assumed to be much greater than its thickness H which, in turn, is much greater than the dimension of the surface features. The surface relief consists of identical (micrometer-sized) punches which are prisms with a rectangular cross section. The axes of these prisms are parallel to the z axis. The punches are equally spaced with spacing $2w$ along the x axis. Let h be the height of a typical punch and $2a$ be its width. Our assumptions are

$$H/D \ll 1 \quad h/H \ll 1 \quad a/H \ll 1 \quad w/H \ll 1 \quad (1)$$

The number of punches per unit length in the x direction, N , is related to the width and spacing of the punches by

$$N = \frac{1}{2(a + w)} \quad (2)$$

The above geometry allows us to consider two-dimensional deformations independent of the out-of-plane (z)

(6) Schmid, H.; Michel, B. *Macromolecules* **2000**, *33*, 3042.

(7) Folch, A.; Schmidt, M. A. *J. Microelectromech. Syst.* **1999**, *8* (1), 85.

(8) Rogers, J. A.; Paul, K. E.; Whitesides, G. M. *J. Vac. Sci. Technol.* **1998**, *B16* (1), 88.

direction. We assume that the applied loads do not vary along the z axis. Since the load does not vary along the prism axes, it is convenient to cast the results in terms of load per unit length (along z). All loads in this work, unless otherwise specified, are defined per unit length in the z direction and have dimensions of force/length. Furthermore, most of the problems in this paper are described by the plane strain theory of elasticity⁹ since the strain along z is zero. We denote the Cartesian component of the Cauchy stress tensor by σ_{ij} . The subscripts i and j take on values 1 and 2 because of the plane strain assumption. Similarly, displacements in the x and y directions are denoted by u_1 and u_2 , respectively.

Often, a stiff (e.g., glass) layer is bonded to the elastomer to provide dimensional stability (see Figure 1). The thickness of the stiff layer is denoted by H_g . We shall assume that H_g is much less than the lateral dimensions of the stamp, D . Young's modulus and the Poisson ratio of the glass layer will be denoted by E_g and ν_g , respectively. The elastomer is assumed to be homogeneous and isotropic with Young's modulus E and Poisson's ratio ν . Most elastomers are incompressible, with $\nu \approx 0.5$ and E between 0.1 and 10 MPa.

In the undeformed configuration, the punches are in incipient contact with the surface of the rigid substrate (the xz plane). Let the top surface of the glass layer be depressed uniformly by an amount $\Delta < 0$. Corresponding to this displacement is a compressive stress, $\sigma_{22} = \sigma_\infty < 0$, acting on the top surface of the glass layer. The remote stress, σ_∞ , is related to the compressive load P acting on a punch by

$$P = \sigma_\infty / N = 2(a + w)\sigma_\infty \quad (3)$$

Δ is related to σ_∞ by

$$\Delta = C_\infty \sigma_\infty \quad (4a)$$

where C_∞ is the compliance,

$$C_\infty = \frac{(1 + \nu)(1 - 2\nu)H}{E(1 - \nu)} \quad (4b)$$

The factor $(1 - 2\nu)/E$ in (4b) is $1/3$ the reciprocal of the bulk modulus, which becomes much larger than the Young's modulus as the material approaches an incompressible state. The compliance is not $1/E$ because of the constraint of the glass layer on the in-plane (xz plane) deformation. Assume that the backing on the elastomer layer is sufficiently stiff, and since σ_∞ is on the order of the modulus of the elastomer or lower, we can also safely neglect the in-plane deformation of the glass due to Poisson expansion, that is, $\nu_g \sigma_\infty / E_g < \nu_g E / E_g \approx 0$. The elastomer layer is therefore subjected to a biaxial stress state with $\sigma_{11} = \sigma_{33} = \nu \sigma_\infty / (1 - \nu) \approx \sigma_\infty$. Thus, the elastomer layer is practically under pure compression σ_∞ except near the edges, where shear stresses occur between the glass/elastomer interface and near the punches. Note that in the absence of a glass layer (or if the glass/elastomer interface cannot support shear), the in-plane strain of the elastomer stamp is $\nu \sigma_\infty / E$ if the contact between the stamp and substrate is frictionless. Since $E_g / E \gg 1$, the in-plane stretching of a stamp bonded to a glass backplane can be several orders of magnitude lower than that of a stamp without a backplane.

Equation 4b is valid only if

$$\lambda \equiv \sqrt{\frac{3(1 - 2\nu)D}{(1 - \nu)H}} \gg 1 \quad (4c)$$

If this condition is not met, then the compliance is given by¹⁰

$$C = C_\infty \left[1 - \frac{\nu^2}{(1 - \nu)^2} \frac{2I_1(\lambda)}{\lambda I_0(\lambda) - \frac{1 - 2\nu}{1 - \nu} I_1(\lambda)} \right]^{-1} \quad (4d)$$

where I_1 and I_0 are modified Bessel functions of order one and zero, respectively. It can be easily demonstrated that (4d) reduces to (4b) for $\lambda \gg 1$.¹⁰

The deformation of the glass layer and the punches in the y direction is neglected in (4). This is because the deformation of the glass layer in this direction is $\approx \sigma_\infty H_g / E_g$ which is several orders of magnitude less than $\sigma_\infty H / E$. The deformation of the punches are of order

$$\frac{Ph}{2aE} = \frac{(a + w)\sigma_\infty h}{aE} \quad (5)$$

which is also much less than $\sigma_\infty H / E$ since $H \gg h$. Note, however, that for a nearly incompressible material ($\nu \approx 1/2$) eq 4c may not be satisfied, and punch deformation may contribute to the overall compliance. Also, we have assumed that w and a are of the same order. If $w \gg a$, then contact between the roof of the stamp and the substrate can occur (see section 3 below).

3. Shape Stability Criteria

Consider first the case of small aspect ratios where $h/a \ll 1$. Since typically $w \approx a$, we also have $h/w \ll 1$ (Figure 2b). The goal is to determine conditions for unwanted contact between the roof of the stamp and the substrate. For this sake, we compute the maximum downward displacement, $(u_2)_{\max} \equiv v_{\max}$, of the surfaces between the punches (roofs) when the stamp is subjected to remote stress, σ_∞ . These roofs are located at $y = h$ and $(2k - 1)w + 2ka < x < (2k + 1)w + 2ka$, where k is any integer (see Figure 1). Symmetry dictates that maximum roof displacement occurs at $x = 2k(w + a)$. Contact of the roof to the substrate occurs when the maximum displacement of the roof equals $-h$. Once this occurs, all surfaces of the stamp (not only the raised punches) can be deformed into contact with the substrate due to surface adhesive forces near the edge of contact.¹¹

The boundary conditions for the problem are

$$\sigma_{12}(x, y = h) = 0 \text{ and } \sigma_{22}(x, y = h) = 0 \\ (2k - 1)w + 2ka < x < (2k + 1)w + 2ka \quad (6)$$

$$\sigma_{12}(x, y = 0) = 0 \text{ and } u_2(x, y = 0) = 0 \quad \text{all other } x \quad (7)$$

$$\sigma_{22}(x, y = H) = \sigma_\infty \text{ and } \sigma_{12}(x, y = H) = 0 \quad \text{for all } x \quad (8)$$

Since $h/a \ll 1$, the maximum displacement v_{\max} can be estimated by replacing the boundary condition in (6) by

(10) Lin, Y. Y.; Hui, C. Y.; Conway, H. D. *J. Polym. Sci., Part B: Polym. Phys.* **2000**, *38*, 2769.

(11) Johnson, K. L.; Kendall, K.; Roberts, A. D. *Proc. R. Soc. London, Ser. A* **1971**, *324*, 301.

(9) Muskhelishvili, N. I. *Some Basic Problems of the theory of Elasticity*; Nordhoff: Groningen, The Netherlands, 1951; translated from Russian by J. R. M. Radok.

$$\sigma_{12}(x, y = 0) = 0 \text{ and } \sigma_{22}(x, y = 0) = 0 \quad (9)$$

Also, because $a/H \ll 1$, $w/H \ll 1$, (8) can be replaced by

$$\sigma_{22}(x, y = \infty) = \sigma_{\infty} \text{ and } \sigma_{12}(x, y = \infty) = 0 \quad (10)$$

This resulting geometry is that of a series of coplanar and periodic cracks. The partial differential equations of plane strain elasticity that govern the solution of this problem can be found in ref 9. The exact solution of these equations subjected to the boundary conditions (9), (10), and (7) can be found in ref 12. Using this solution, the maximum vertical displacement at $x = 2k(w + a)$ is

$$v_{\max} = \frac{4\sigma_{\infty}}{\pi E^*} (w + a) \cosh^{-1} \left[\sec \left(\frac{w\pi}{2(w + a)} \right) \right] \quad (11)$$

where $E^* \equiv E/(1 - \nu^2) \approx 4E/3$. The accuracy of (11) will be tested against finite element method (FEM) results in section 6. Equation 11 can be simplified when the roofs are far apart, that is,

$$v_{\max} = \frac{2\sigma_{\infty} w}{E^*} \quad w/a \ll 1 \quad (12)$$

According to (11), to prevent the contact of roofs, the condition

$$\frac{2\kappa_1}{\pi} \left(1 + \frac{a}{w} \right) \cosh^{-1} \left[\sec \left(\frac{w\pi}{2(w + a)} \right) \right] < 1 \quad (13a)$$

must be satisfied (the negative sign accounts for $\sigma_{\infty} < 0$ for compressive stresses), where $\kappa_1 \equiv -2\sigma_{\infty} w/E^* h$. Equation 13a implies that the contact condition is determined by two dimensionless parameters, κ_1 and w/a . If the roofs are far apart, then (13a) reduces to

$$\kappa_1 \approx \frac{-2\sigma_{\infty} w}{E^* h} < 1 \quad (13b)$$

The dependence of the contact condition $v_{\max} = -h$ on w/a is plotted in Figure 3. The vertical axis of Figure 3 is κ_1 and the horizontal axis is w/a . For small w/a , it is clear that κ_1 approaches 1. The roofs of stamps with parameters (κ_1 , w/a) lying below the curve in Figure 3 will not contact.

We next establish criteria for buckling of the stamp. It is anticipated that buckling occurs when $h \gg a$. The critical buckling load P_c depends on the support conditions assumed for the punch at its two ends. We assume the punch to be clamped where it meets the main stamp and simply supported at its contact with the substrate, consistent with frictional restraints. Then,¹³

$$P_c \approx \frac{1.36\pi^2 E^* a^3}{h^2} \quad (14)$$

Using (3) and (14), buckling will not occur if the condition

$$\kappa_2 = -\frac{1.47\sigma_{\infty} h^2}{\pi^2 E^* a^2} < \frac{1}{1 + (w/a)} \quad (15a)$$

is satisfied. The constant (~ 1.47) in this expression for critical buckling load is very sensitive to the boundary conditions. For this reason, we would suggest that eq 15a

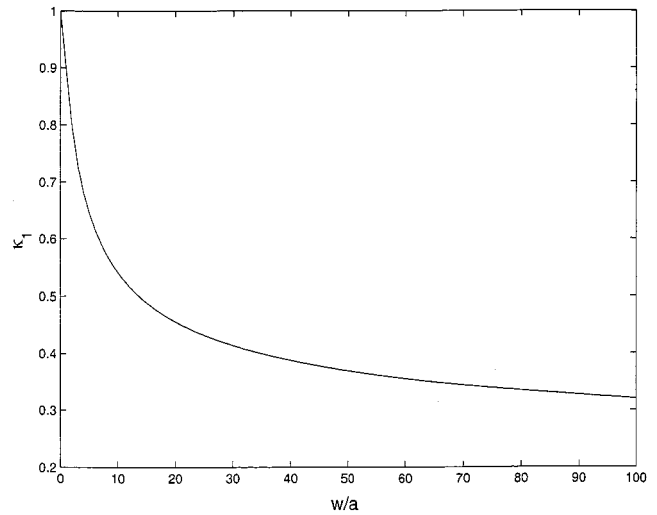


Figure 3. The condition of contact of the stamp roof with the substrate can be expressed in terms of two dimensionless parameters $\kappa_1 = -\sigma_{\infty} w/(E^* h)$ and w/a . Points lying below the curve will not satisfy the contact condition.

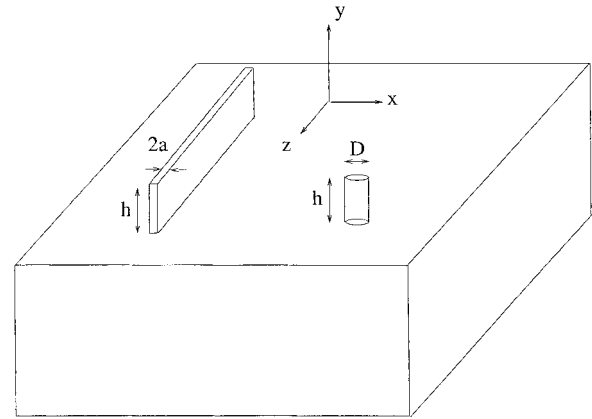


Figure 4. Geometry of a two-dimensional platelike punch and a prism-shaped punch.

be regarded more as a scaling relationship than an exact result. As an example, the load on a punch due to the weight of the elastomer alone is $2\rho g H(a + w)$, where ρ is the mass density and $g = 9.81 \text{ m/s}^2$. For $a = w$, buckling can occur when $h/a = (\pi/2)[1.36E^*/(\rho g H)]^{1/2}$.

The above analysis focuses on buckling of the punches during stamping, where a compressive stress is applied. A similar analysis can be carried out to quantify the experimental results of Biebuyck et al.³ Their experiments showed that isolated two-dimensional platelike punches (see Figure 4) are stable under their own weight for $2a/h$ as large as 10. However, cylindrical punches with circular cross sections (with diameter d) and height h collapsed under their own weight when $h/d \approx 6$ (see Figure 4).

The critical height for the buckling of a column of arbitrary cross sections under its own weight can be found in ref 13; it is

$$h_c = (7.837EI/q)^{1/3} \quad (15b)$$

where $I = \pi d^4/64$ for a circular cylinder and $q = \rho g \pi d^2/4$ is the weight per unit length of the cylinder. For a long rectangular plate of height h and width $2a$, the critical buckling height is still given by (15b) provided that E is replaced by E^* , $I = (2a)^3/12$, and $q = 2\rho g a$. The ratio of the critical heights for the plate and the cylinder is

(12) Koiter, W. T. *Ing. Arch.* **1959**, *28*, 168.

(13) Timoshenko, S. P.; Gere, J. M. *Theory of Elastic Instability*, 2nd ed.; McGraw-Hill: New York, 1961.

$$h_c^{\text{plate}}/h_c^{\text{cyl}} = \left(\frac{4(2a)^2}{3(1-\nu^2)d^2} \right)^{1/3} \quad (15c)$$

In Biebuyck et al.'s experiments,³ $2a = d = 1 \mu\text{m}$ so that this ratio is about 1.2 where we have assumed $\nu = 0.5$. This result is in qualitative agreement with the experimental results of ref 3. According to (15b), the plates should buckle when $h/d \approx 7.3$, given the buckling condition for a cylinder. Thus, (15b) predicts a lower critical height for plate buckling compared with the experimental data. Quantitative predictions of buckling load are known to be extremely sensitive to imperfections, load-sharing, and particularly the support boundary conditions; the discrepancy likely arises among one of these.

To establish a criterion for lateral stability, consider the situation depicted in Figure 2a, where two neighboring punches adhere to each other. Let l be the length of the noncontact region. In the contact region, the plates are virtually undeformed. In other words, all the elastic strain energy is stored in the noncontact region, where bending deformation is dominant. The total strain energy SE of the system can be easily computed using elementary plate theory, assuming that the punches are plates clamped at one end, that is,

$$\text{SE} = \frac{16E^*a^3w^2}{l^3} \quad (16)$$

As expected, for a given w , the elastic strain energy decreases with increasing l . Suppose the straight edge separating the contact and the noncontact region in Figure 2b advances a small amount dl , that is, $l \rightarrow l + dl$. The resulting decrease in strain energy is

$$d\text{SE} = -\frac{48E^*a^3w^2}{l^4}dl \quad (17)$$

Under equilibrium conditions, this energy change equals the amount of work dW needed to decrease the contact area by dl . If we denote the surface energy by γ_s , $dW = 2\gamma_s dl$. Therefore, we must have

$$l = 2 \left[\frac{3E^*a^3w^2}{2\gamma_s} \right]^{1/4} \quad (18)$$

From the above discussion, it is clear that punches with height less than l will be laterally stable. Thus, the condition for lateral stability is

$$\frac{2 \left[\frac{3E^*a^3w^2}{2\gamma_s} \right]^{1/4}}{h} > 1 \quad (19a)$$

or

$$\kappa_3 \equiv \frac{h \left[\frac{2\gamma_s}{3E^*a} \right]^{1/4}}{2a} < \sqrt{w/a} \quad (19b)$$

4. Shape Change Imposed by Surface Tension

Surface tension forces will deform the molded sharp corners of the punches into a smooth equilibrium shape after these punches are released from the master. For fine features in soft stamps, the scale of the deformation may be significant. In this section, we determine the internal stresses and deformation generated by surface tension.

For mathematical simplicity, we confine ourselves to studying local deformation in the vicinity of a corner. The

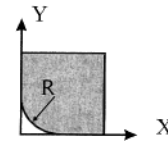


Figure 5. Rounded corner of a stamp with radius of curvature R .

corner coincides with the origin of the xy plane (see Figure 5). Let (r, θ) be a polar coordinate system with the same origin. The corner can be generated by a sequence of quarter circles with decreasing radius R_n such that

$$R_n \rightarrow 0 \quad n \rightarrow \infty$$

Assume a constant, isotropic surface tension. The Laplace pressure p due to surface tension vanishes everywhere except on the circle, where

$$p = \gamma_s/R_n \quad (20)$$

The total load acting on the arc of the quarter circle is $\sqrt{2}\gamma_s$, which is independent of the radius R_n . Thus, in the limit $R_n \rightarrow 0$, the effect of surface tension is represented by a concentrated compressive line force of magnitude $\sqrt{2}\gamma_s$, acting at an angle that bisects the corner.

We have thus reduced the problem to one in the theory of plane strain elasticity. The boundaries are traction-free conditions on the surfaces $y = 0, x > 0$ and $x = 0, y > 0$. Specifically,

$$\sigma_{12} = \sigma_{22} = 0 \quad y = 0, x > 0 \quad (21a)$$

$$\sigma_{21} = \sigma_{11} = 0 \quad x = 0, y > 0 \quad (21b)$$

The origin is a singular point where the concentrated load acts. The exact solution can be obtained using the complex function method of Muskhelishvili.⁹ The stresses are

$$\sigma_{11} = \frac{\sqrt{2}\gamma_s}{(\pi + 2)r} \left(2 \cos\left(\frac{\pi}{4} - \theta\right) + \cos\left(\frac{\pi}{4} + \theta\right) + \cos\left(\frac{\pi}{4} - 3\theta\right) \right) \quad (22a)$$

$$\sigma_{22} = \frac{\sqrt{2}\gamma_s}{(\pi + 2)r} \left(2 \cos\left(\frac{\pi}{4} - \theta\right) - \cos\left(\frac{\pi}{4} + \theta\right) - \cos\left(\frac{\pi}{4} - 3\theta\right) \right) \quad (22b)$$

$$\sigma_{12} = \frac{\sqrt{2}\gamma_s}{(\pi + 2)r} \left(-\sin\left(\frac{\pi}{4} - 3\theta\right) + \sin\left(\frac{\pi}{4} + \theta\right) \right) \quad (22c)$$

The displacements, u_1 and u_2 , are

$$u_1 = \frac{(1 + \nu)\sqrt{2}\gamma_s}{E} \ln r + c_1 \quad (22d)$$

$$u_2 = \frac{(1 + \nu)\sqrt{2}\gamma_s}{E} \ln r + c_2 \quad (22e)$$

where c_1 and c_2 are arbitrary constants.

According to (22a–c), the stresses are proportional to the surface energy and have a $1/r$ singularity as the corner is approached. The displacement fields also have a weak logarithmic singularity and are proportional to γ_s/E , which is the only length scale in the problem. The reason that

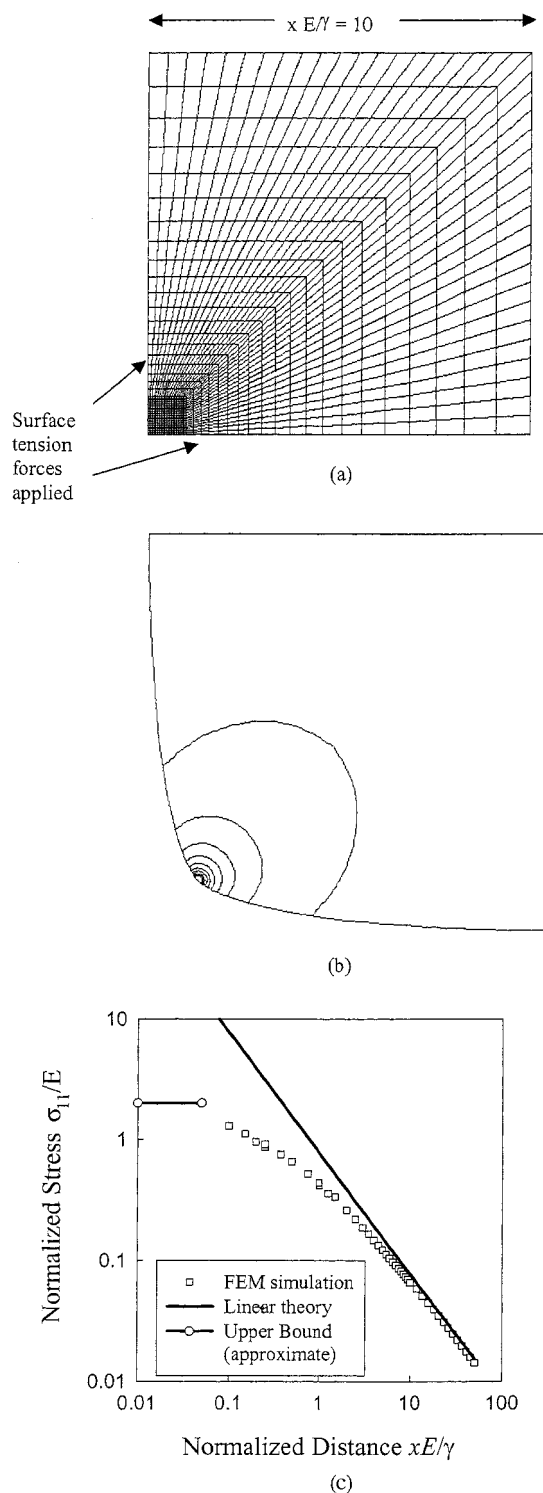


Figure 6. (a) Finite element mesh. (b) Contours of P/E , where P is pressure. Contour furthest from the rounded edge represents a value of 0.1. Contour steps are 0.1 each; the maximum value is 1.87, implying a rounded radius $R \approx 2\gamma_s E$. (c) Normalized stress, σ_{11}/E , as a function of normalized distance from corner, $x E/\gamma$, along the positive x axis. The solid line is the analytical approximation (22a). There is good agreement between the two at distances greater than $x \approx \gamma_s/E$. Close to the corner, the linear analytic theory predicts unbounded stresses. In the simulation, stress is bounded due to finite change in geometry. If the deformed radius is $\sim \gamma_s/E$, the maximum stress is $\sigma/E \sim 2.0$, shown by the solid line.

these singularities exist is because the problem is inherently nonlinear and the solution is based on linear theory. Specifically, our solution calculates the shape change due

to a concentrated force. It does not take into account the fact that the force distribution (not the total force) alters with shape change. Specifically, deformation causes the Laplace pressure to be no longer concentrated and hence singular. The final equilibrium shape is one that minimizes the total energy (elastic strain energy and surface energy) of the system. Our solution can be expected to be valid in regions close to but not exactly at the corner.

To justify the linear analysis, detailed nonlinear finite element simulations of surface tension induced deformations have been carried out using the commercial finite element package, ABAQUS.¹⁴ The finite element model allows for large deformation as well as nonlinear elastic behavior. Furthermore, the geometry is continually updated to accommodate changing surface forces. The stamp was modeled as an hyperelastic neo-Hookean material; its geometry was discretized using 4-node quadrilateral elements (Figure 6a). To compare with the linear theory, the tensile behavior of the neo-Hookean material at small strains is chosen to be identical to the linear theory. The only driving force for deformation in this problem, surface tension, has been applied via a user element that provides contributions to the global nodal forces and stiffness.¹⁵

Parts a and b of Figure 6 show the initial, undeformed finite element mesh and the deformed shape with contours of pressure, normalized by the Young's modulus, respectively. In the simulation, the stresses remain finite, with a maximum value of ~ 1.9 . Because near the corner the pressure is related to deformed radius, r , as $P \sim \gamma_s/r$, this confirms the scaling prediction that a sharp corner is rounded to a radius of about $r \sim \gamma_s/E$.

Figure 6c plots $-\sigma_{11}(x,0)/E$ as predicted by the analytic solution and the simulation. There is good agreement between the two for distances larger than $\sim \gamma/E$. At the corner, the small-strain analytic solution is singular. Consistent with the discussion of the previous paragraph, the numerically computed stress is bounded, roughly by $\sigma/E < 1$.

Our analysis shows that surface tension forces will deform the molded sharp corners of the punches into a smooth equilibrium shape with a radius of curvature on the order of γ_s/E after these punches are released from the master. Thus, γ_s/E represents a lower limit for the radius of curvature of corners. For PDMS, γ_s/E is on the order of $0.05 \mu\text{m}$.

5. Residual Stresses in the Stamp Due to Thermal and Chemical Shrinkage

The residual stresses in the glass and elastomer layer can be obtained by treating the thermal and chemical shrinkage as transformation strains.¹⁶ The problem is analogous to the internal stresses generated in thin films on substrates during deposition.¹⁷ The original flat, layered structure bends into a shell with constant radius of curvature R . Taken positive as concave up, R is found to be¹⁶

$$R = \frac{(1 + \omega\delta)\gamma H_g}{12\Delta\epsilon_T(1 + \gamma\chi)} \quad (23a)$$

where

(14) Hibbit, Karlsson & Sorensen, Inc.: Pawtucket, RI.

(15) Jagota, A.; Argento, C.; Mazur, S. *J. Appl. Phys.* **1998**, 83 (1), 250.

(16) Hui, C. Y.; Lin, Y. Y.; Conway, H. D. *J. Electron. Packaging* **2000**, 122, 267.

(17) Nix, N. D. *Metall. Trans.* **1989**, 20A, 2217.

$$\omega = E_g/E \quad \delta = H_g/H \quad (23b)$$

$$\gamma = \frac{\omega\delta^2(1+\delta)}{2(1+\omega\delta^3)} \text{ and } \chi = \frac{6(1+\delta)}{\delta(1+\omega\delta)} \quad (23c)$$

$$\Delta\epsilon_T = (\alpha - \alpha_g)(T - T_c) + \epsilon_s \quad (23d)$$

$$E' = E/(1 - \nu) \quad E'_g = E/(1 - \nu_g) \quad (23e)$$

α and α_g are the thermal coefficients of expansion of the elastomer and the glass, respectively, T is the ambient temperature, T_c is the curing temperature of the elastomer, and $\epsilon_s < 0$ is the shrinkage strain of the elastomer as a result of curing.

The stress state in the glass and elastomer layer is biaxial; that is, $\sigma_{11} = \sigma_{33} \equiv \sigma$ are the only nonvanishing stress components. The biaxial stresses are uniform in the x and z direction and are linear in the y direction. It is given in ref 16 that

$$\sigma_g = \frac{E'_g \Delta\epsilon_T}{(1 + \omega\delta)(1 + \gamma\chi)} \left[1 + \frac{12\gamma y_g}{H_g} \right] \quad |y_g| \leq H_g/2 \quad (24a)$$

$$\sigma = \frac{E'_g \Delta\epsilon_T}{(1 + \omega\delta)(1 + \gamma\chi)} \left[-\delta + \frac{12\gamma y}{\omega H} \right] \quad |y_e| \leq H/2 \quad (24b)$$

where σ_g and σ are the biaxial stresses in the glass and elastomer layer, respectively. y_g and y_e are coordinates normal to the plane of each layer (measured positive down from the center of each layer) as shown in Figure 7. For example, the interface between the glass and polymer layer is located at $y_g = H_g/2$ or $y_e = -H/2$. If the elastomer layer is much thinner than the glass layer ($\delta \gg 1$) or if the glass layer is much stiffer than the elastomer ($\omega \gg 1$), then (24a) and (24b) reduce to

$$\sigma \cong -E' \Delta\epsilon_T \quad (25a)$$

$$\sigma_g \cong E' \Delta\epsilon_T H/H_g \quad (25b)$$

The radius of curvature in this limit is called the Stoney formula:¹⁸

$$R = \frac{\omega\delta H_g}{24\Delta\epsilon_T} \quad (25c)$$

Since the elastomer modulus is ≈ 1 MPa whereas the substrate, say glass, has a modulus of ≈ 100 GPa, $\omega \approx 10^5$, (25a,b) are typically excellent approximations. In particular, the biaxial stresses in the glass and elastomer layer are uniform. The fact that the stress in the elastomer layer is uniform when $H/D \ll 1$ was observed by the finite element simulations by Rogers et al.⁸ The above analysis breaks down when H and D are comparable. In this case, material points close to the top free surface of the elastomer can contract freely, whereas material points close to the elastomer/glass interface have practically no in-plane (xz) deformation. In this case, the in-plane displacement of the elastomer layer will be inhomogeneous in both the x and y directions, as noted in ref 8.

Equation 23a showed that stamps with prescribed radii of curvature could be made by choosing appropriate values for ω and δ .

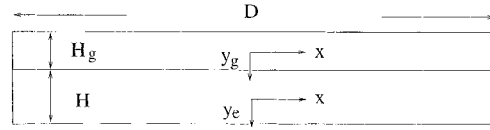


Figure 7. Definition of local coordinate system y_g and y_e . It is assumed that $D \gg H, H_g$. The punches are not shown in this figure.

6. Contact Stresses

In this section, we estimate the contact pressure beneath the punches. In the following, we will adopt the standard contact mechanics approach by assuming that the contact surfaces are frictionless so that slip (discontinuity in tangential displacements) can occur between the contacting surfaces. Note that the frictionless boundary condition does not necessarily imply slip; it merely implies that slip can occur. In practice, it is very difficult to slide the PDMS against the substrate, so that the no-slip boundary condition is much more appropriate. However, for the case of PDMS against a rigid substrate, the frictionless boundary condition is justified because of the following result in contact mechanics:¹⁹ the no-slip condition is satisfied for frictionless contact between two surfaces if one of the materials is rigid (e.g., the substrate) and the other incompressible (i.e., $\nu = 0.5$). Specifically, for an incompressible material (e.g., the elastomeric stamp) contacting a frictionless rigid surface, the tangential displacement of the soft material (the elastomer) is zero so that the no-slip is satisfied. Since the PDMS is typically much softer than the substrate and its Poisson's ratio is close to $1/2$, the frictionless boundary condition is equivalent to the no-slip condition. This result seems to be counter-intuitive since one may think that because the punch is compressed at constant volume, it must expand laterally. However, because the elastomeric punches are very small in comparison to the layer of elastomer they are attached to, this mental picture is not accurate and indeed the lateral displacement, even under no-slip boundary conditions, is negligible.

Consider first the case of small aspect ratios, where $h/a \ll 1$. In this limit, the Hertz approximation²⁰ is applicable, in which the contact stresses are estimated by replacing the elastomer by a half space. On the boundary of this half space, that is, $y = 0$, the following boundary conditions are imposed:

$$\begin{aligned} u_2(x, y = 0) &= \Delta & x \in \Omega \\ \sigma_{22}(x, y = 0) &= 0 & x \notin \Omega \\ \sigma_{12}(x, y = 0) &= 0 & \text{for all } x \end{aligned} \quad (26)$$

where Ω is the set of all x satisfying $(2k - 1)a + 2kw < x < (2k + 1)a + 2kw$ where k is an integer (see Figure 8).

The pressure distribution $p(x)$ beneath the punches is obtained using the complex function method of Muskhelishvili.⁹ Details of the solution method can be found in ref 21. The result is

(19) Johnson, K. L. *Contact Mechanics*; Cambridge University Press: Cambridge, 1985.

(20) Hui, C. Y.; Baney, J. M.; Lin, Y. Y. In *Adhesion Measurement of Films and Coatings*; Mittal, K. L., Ed.; VSP BV: Utrecht, The Netherlands, 2001; Vol. 2, pp 299–328.

(21) Hui, C. Y.; Lin, Y. Y.; Baney, J. M.; Kramer, E. J. *J. Polym. Sci., Part B: Polym. Phys.* **2001**, *39*, 1195.

(18) Stoney, G. G. *Proc. R. Soc. London, Ser. A* **1909**, *82*, 172

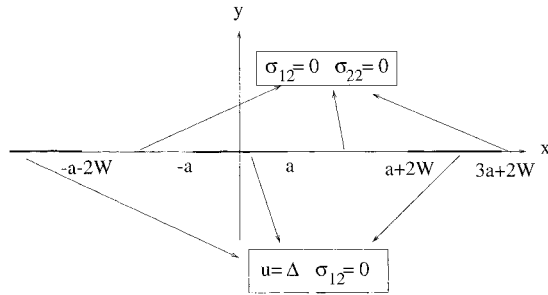


Figure 8. Geometry and boundary conditions in the contact problem.

$$p(x) = \frac{P}{2(a+w)} \cos\left(\frac{\pi x}{2(a+w)}\right) \left[\sin^2\left(\frac{\pi a}{2(a+w)}\right) - \sin^2\left(\frac{\pi x}{2(a+w)}\right) \right]^{-1/2} \quad (27)$$

where P is the load on a punch. If the punches are spaced far apart, that is, $a/w \ll 1$, the above solution reduces to the solution of a rigid punch indenting on a elastic half space, that is,

$$p(x) = \frac{P}{\pi \sqrt{a^2 - x^2}} \quad (28a)$$

Note that the pressure distributions in (27) and (28a) have square root singularities at the edges of the punch. Indeed, as $x \rightarrow a$, (28a) implies that

$$p(x \rightarrow a) \rightarrow \frac{P}{\pi \sqrt{2a}} (a - x)^{-1/2} \quad (28b)$$

Note that the strength of this singularity is $k_\infty = P/\pi\sqrt{2a}$ when the punches are widely spaced. For the general case, (27), the strength of the singularity, k , can be obtained by taking the limit of $x \rightarrow a$ and is

$$k = \frac{P}{2\sqrt{\pi(a+w)}} \sqrt{\cot \pi n \left(\frac{\pi a}{2(a+w)} \right)} \quad (28c)$$

The effect of spacing on the strength of the stress singularity can be examined by considering the ratio k/k_∞ which is plotted in Figure 9. This ratio approaches 1 and 0 as $w/a \rightarrow \infty$ and 0, respectively. Furthermore, it is independent of P . As expected, the stress concentration decreases with decreasing w/a . The limit $w/a \rightarrow 0$ corresponds to two flat surfaces in contact so that there is no stress concentration.

The presence of the square root singularity is due to the Hertz approximation. If the exact boundary conditions are used, the pressure distribution is bounded but will be very large at the edge, provided that the aspect ratios are small.

Note that the work of adhesion W_{ad} between the polymer/substrate interface does not appear in the above solution. This is because the punches are assumed to be perfectly flat as well as to have right angle corners. The connection between adhesion and contact pressure can be clarified by approximating the perfect rectangular profile of the punch by a smooth curve (see (29) below). Since the stress concentration is most severe when the punches are spaced far apart, we focus on a single punch, ignoring interaction effects. The profile of a "perfect" punch can be approximated by the smooth function

$$f(x) = h(x/a)^{2n} \quad (29)$$

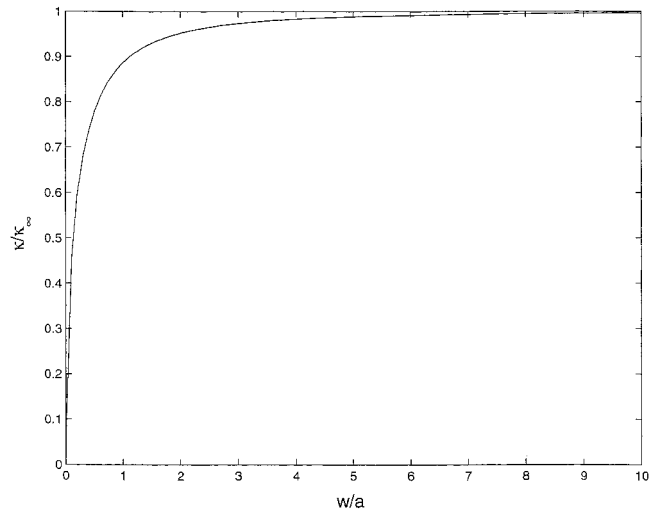


Figure 9. The strength of the pressure near the edge of the contact zone can be expressed in terms of k/k_∞ . The dependence of k/k_∞ on the spacing w/a is shown.

where n is a large positive integer. Since n is large, $f(x)$ is practically zero for $x < a$ (i.e., the punch is almost flat). For example, for $x = 0.9a$, $(x/a)^{2n} = 2.7 \times 10^{-5}$ for $n = 10$. On the other hand, $f(x = 1) = h$ for all n . As x approaches a (i.e., the corner), for example, $x \approx e^{-1/(2n)}a$, the function increases extremely rapidly to h .

Suppose an elastic punch with this profile is brought into contact with a rigid substrate. Let P be the force on the punch and $2b$ be the contact width. We seek the relation between P and b . The pressure distribution underneath the punch can be found using a result of Muskhelishvili⁹ and is

$$p(x) = \frac{E^* h (b/a)^{2n}}{2\pi} \frac{I_n(x)}{\sqrt{b^2 - x^2}} + \frac{P}{\pi \sqrt{b^2 - x^2}} \quad (30a)$$

where

$$I_n(x) = 2n \text{PV} \left[\int_{-1}^1 \frac{\sqrt{1-u^2} u^{2n-1} du}{-u + (x/b)} \right] \quad (30b)$$

and PV denotes a principal value integral. Equation 30a implies that the pressure has an inverse square root singularity as the edge of the contact zone is approached. For example,

$$p(x) \rightarrow \frac{K_I}{\sqrt{2\pi(b-x)}} \quad x \rightarrow b \quad (30c)$$

where

$$K_I = \frac{E^* h (b/a)^{2n}}{2\sqrt{\pi} b} I_n(b) + \frac{P}{\sqrt{\pi} b} \quad (30d)$$

The integral $I_n(b)$ is found to be $2n\pi(2n)!/[2^{2n}(n!)^2] \approx 2\sqrt{n\pi}$ using a contour integration technique and Sterling's approximation. To determine the contact length, we use the Johnson–Kendall–Roberts (JKR) theory.^{11,20} In this theory, the region exterior to the punch and the substrate is treated as an external crack. The amount of strain energy released when this external crack increases by db is $db K_I^2/2E^*$ (i.e., the contact edge at b decreases by db). In equilibrium, the energy needed to separate the interface by db is $W_{ad} db$. Therefore,

$$K_I = \sqrt{2E^*W_{ad}} \quad (31)$$

Combining (30d) and (31), we have

$$\frac{E^*h\sqrt{n}\left(\frac{b}{a}\right)^{2n}}{\sqrt{b}} + \frac{P}{\sqrt{\pi b}} = \sqrt{2E^*W_{ad}} \quad (32)$$

If W_{ad} is known, the dependence of the contact length on load is completely determined by (32). For $b/a < 1$, the first term in the left-hand side (LHS) of (32) is very small compared with the second term, so that

$$P \cong \sqrt{2\pi bE^*W_{ad}} \quad (33)$$

Note that P is positive, so that equilibrium can be maintained if the punch is subjected to a *tensile* force. This is because the adhesive surface forces acting on the punch must be balanced by an upward tensile force. If the applied load is zero, (32) predicts that the punch will spontaneously jump into contact with the substrate until

$$b = \left(\frac{2W_{ad}a^{4n}}{nE^*h^2} \right)^{1/(4n-1)} \quad (34)$$

For large n , the right-hand side (RHS) of (34) is close to but slightly less than a . This result is not surprising: if the punch and substrate surfaces were perfectly flat, perfect contact would occur with no applied load. In other words, a compressive load ($P < 0$) would not be necessary for good contact were it not for surface roughness.

Finally, we note that when $b = a$ the first term on the LHS of (32) becomes very large since it is proportional to \sqrt{n} . In this case the RHS of (32) can be neglected and

$$P = E^*h\sqrt{n\pi} \quad (35)$$

The interpretation is clear: a compressive load is needed to bring the contact length arbitrarily close to a . That this compressive load is arbitrary can be seen by noting that n can be arbitrarily large in (35).

The analysis above assumes that the aspect ratio $h/a \ll 1$. As h/a increases, these solutions are no longer valid since the pressure distributions underneath the punches will become more uniform. Indeed, for sufficiently large h/a , the pressure is expected to be uniformly distributed, that is, $p(x) = P/2a$. From linearity and dimensional analysis, the pressure distribution must have the form

$$p(x) = \sigma_\infty \phi(x/a, h/a, w/a, \nu) \quad (36)$$

Note that the normalized pressure $\phi = p/\sigma_\infty$ depends only on the geometry and is independent of the material properties. We carried out finite element simulations to determine ϕ . The elastomer layer is assumed to be perfectly bonded to a rigid backplane so that there is no horizontal displacement along the elastomer/backplane interface. Finite element simulations were carried out in the region $0 \leq x/a \leq 1 + w/a$, $0 \leq y \leq H + h$ since the punches are periodically distributed and symmetrical. By symmetry, the shear traction vanishes on the lines $x = 0, 0 \leq y \leq H + h$ and $x = a + w, 0 \leq y \leq H$. The horizontal displacement on these lines is zero due to symmetry and the lateral constraint of the rigid backplane. The mechanical interaction between the elastomer layer and the rigid backplane is modeled by applying a uniform compressive load $\sigma_{22} = \sigma_\infty$ on the upper boundary $y = H + h, 0 \leq x/a \leq 1 + w/a$.

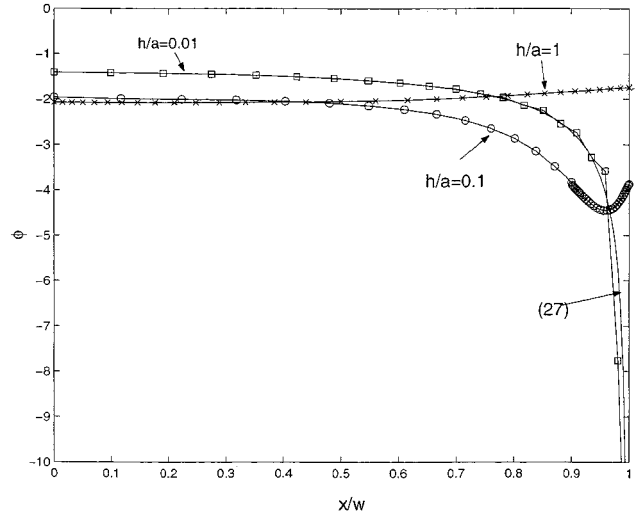


Figure 10. The pressure distribution underneath a typical punch for different aspect ratios h/a . These FEM simulations are carried out with $\nu = 0.48$ and $w/a = 1$.

In addition, the horizontal displacement on this boundary is zero because of the rigid constraint. The punch surfaces at $x = a$ and $x = a + w$ are traction free. Since the punch is pushing against the rigid substrate at $y = 0, 0 \leq x/a \leq 1$, the vertical displacement on this boundary is zero. Finally, there is no shear stress on this boundary due to frictionless contact. The pressure distribution for different aspect ratios is shown in Figure 10. These simulations were carried out with $w/a = 1$ and $\nu = 0.48$ so that the normalized pressure distribution depends only on the aspect ratio h/a . For small aspect ratios, the pressure distribution predicted by (27) should be an excellent approximation. This pressure distribution is plotted in Figure 10. As expected, it agrees almost perfectly with the FEM result for $h/a = 0.01$. For sufficiently small aspect ratios, a region of high pressure should exist near the punch edges. This is demonstrated by our FEM results for $h/a = 0.1$. On the other hand, Figure 10 shows that the pressure distribution is practically uniform for $h/a = 1$. From a force balance, this pressure is $\sigma_\infty(a + w)/a$, or $\phi = -2$ since $a = w$ was used in the simulation. Thus, the contact pressure under the punches with aspect ratio $h/a \geq 1$ is uniform and is equal to $\sigma_\infty(a + w)/a$. These finite element results also allow us to assess the accuracy of the approximate solution (11). The normalized downward displacement $\bar{v} \equiv \pi E^* u_2/4\sigma_\infty(w + a)$ profiles of the roof at $y = h, a < x < a + w$ for three different aspect ratios are shown in Figure 11. The maximum normalized downward displacement computed using FEM compares extremely well with \bar{v}_{\max} (labeled by the symbol *, $h/a = 0.01$, Figure 11) computed using (11). At $h/a = 0.1$, the prediction of (11) is about 20% higher than the FEM results. Therefore, (11) can be used to estimate the maximum downward displacement for $h/a < 0.1$.

7. Surface Roughness

In practice, contact surfaces are not perfectly smooth and compressive loads are needed to bring the surfaces into conformal contact with one another. In this section, a model is used to estimate the force per punch needed to maintain intimate contact in the presence of surface roughness. In what follows, we assume that the roughness is entirely on the stamp. It is important to realize that the rigid substrate can have roughness, often due to the presence of previously deposited devices or circuit lines. The results to be developed below nevertheless hold as

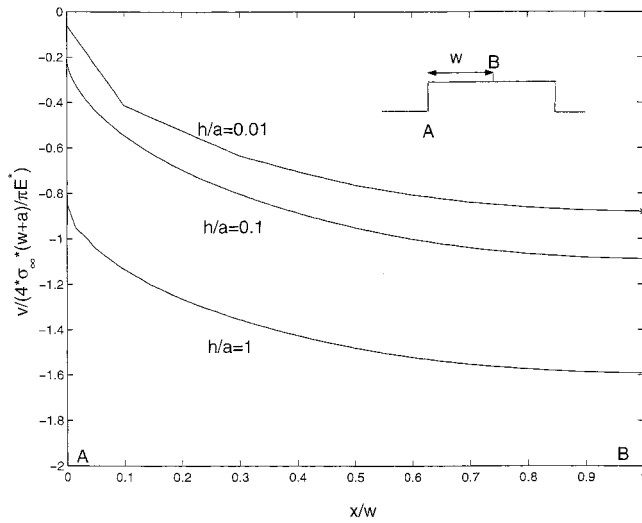


Figure 11. Maximum pressure as a function of aspect ratio h/a . These FEM simulations are carried out with $\nu = 0.48$ and $w/a = 1$. The symbol * on the right-hand side of the graph ($h/a = 0.01$) is \bar{v}_{\max} computed using (11).

long as the roughness profile $f(x)$ below corresponds to the combined roughness of the two surfaces.

The connection between the adhesion of solids and the contact of rough surfaces is well-known. For example, a theory of adhesion based on the contact of random asperities was developed by Greenwood and Williamson²² for elastic bodies in contact. The analysis of Greenwood and Williamson²² does not take into account the interaction of neighboring asperities. Interaction effects were first studied by Johnson,²³ who considered a periodic array of cylindrical asperities of a specific shape and derived the stability condition of the two contact surfaces. By stability, we mean the following: when a rough polymer surface is brought into contact with a rigid flat substrate, the space between asperities shrinks due to the surface deformation by adhesive forces. Under certain conditions, the surfaces can heal without the application of external pressure. Johnson's work has been recently extended by Hui et al.²¹ This work allows for asperities with arbitrary smooth profiles. It also studies the effect of trapped air on the contact mechanics. In the following, the results of this work are used to determine the force per punch needed to maintain intimate contact in the presence of surface roughness.

The rough surface of the "flat" punch is assumed to be much greater than the size of an asperity. Furthermore, the asperities are assumed to be periodically distributed on this surface. To be precise, the surface roughness of the elastomer punch is described by a periodic function $f(x)$ with period L (see Figure 12). Without loss of generality, we assume that $f(x)$ is a non-negative smooth even function of x satisfying $f(x = 0) = 0$. As illustrated in Figure 12, the contact zones consist of many infinitely long strips (in the out-of-plane direction) of width $2c$ located at $(kL - c, kL + c)$, where k is an integer. To be specific, we shall assume that

$$f(x) = h_a \sin^2\left(\frac{\pi x}{L}\right) \quad (37)$$

where h_a is the asperity height. Explicit solution of the general case, including the contact pressure, can be found in ref 21.

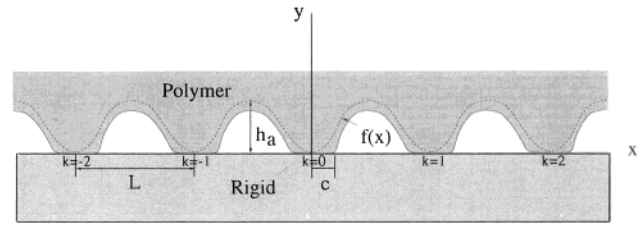


Figure 12. Geometry of the surfaces before (dotted line) and after contact. The surface profile is described by a periodic function $f(x)$ of period L . The contact zones are infinite strips in the out-of-plane direction with width $2c$. The contact zone boundaries are located at $kL \pm c$, where k is an integer. The two surfaces heal when $c = L/2$.

Each punch is compressed by a line force P which is related to the compressive stress acting on the stamp by (3). P is also related to the force per asperity, P_a , by

$$P = N_a P_a \quad (38)$$

where $N_a = 2a/L$ is the total number of asperities on the punch surface. The contact zones are infinite long strips in the z direction with width $2c$. The length of these contact zones must satisfy the geometrical constraint

$$2c < L \quad (39)$$

Finally, we point out that $2c/L$ is also the fraction of area in contact. Perfect contact is achieved when $2c/L = 1$.

The relation between P_a and $2c$ is given in ref 21 as

$$\frac{-2P_a}{\pi E^* h_a} = \sin^2(\pi\eta) - \alpha \sqrt{\tan(\pi\eta)} \quad (40a)$$

where

$$\eta = c/L \quad (40b)$$

is the normalized contact length and

$$\alpha = \frac{2\sqrt{2}}{\pi} \frac{\sqrt{L}}{h_a} \sqrt{\frac{W_{ad}}{E^*}} \quad (40c)$$

is a dimensionless parameter. Note that if we introduce a normalized load per asperity \bar{P}_a given by

$$\bar{P}_a = \frac{2}{\pi E^* h_a} P_a \quad (41)$$

then the normalized contact length is completely determined by the normalized load and the dimensionless parameter α . Recall that the geometrical constraint $2c/L < 1$ restricts the arguments of the trigonometric functions in (40a) to remain in the interval $[0, \pi/2]$. When full contact occurs, that is, as $\eta \rightarrow 1/2$, the second term in (40a) becomes dominant since $\tan(\pi\eta) \rightarrow \infty$. In this limit, equilibrium can be maintained only by the application of a very large tensile P_a (i.e., $P_a > 0$). Therefore, it is possible for the two surfaces to be unstable in a load-controlled test by spontaneously jumping into contact. Figure 13 plots the normalized force $-\bar{P}_a$ versus the normalized contact length η for different values of α . When $\alpha \geq 0.57$, the force in (40a) is tensile for all $2\eta < 1$. This means that if there were no applied load, the surfaces would jump spontaneously. For $\alpha < 0.57$, the surfaces jump spontaneously into

(22) Greenwood, J. A.; Williamson, J. B. P. *Proc. R. Soc. London, Ser. A* **1996**, A295, 300.

(23) Johnson, K. L. *Int. J. Solids Struct.* **1995**, 32 (3/4), 442.

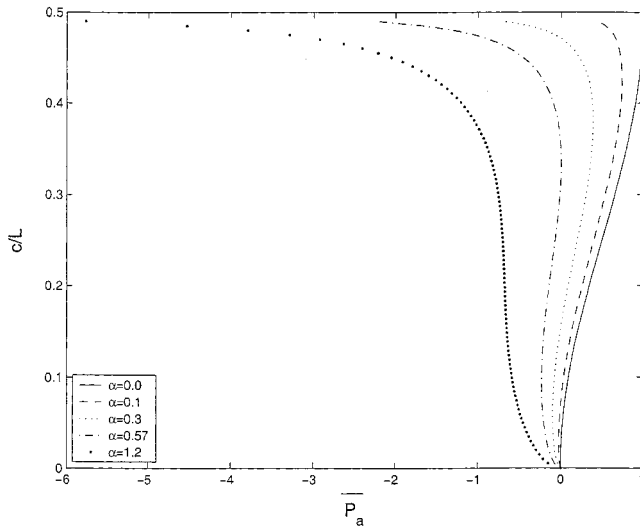


Figure 13. Normalized contact zone length $\eta = c/L$ versus the normalized contact force per asperity $\bar{P}_a = (2/\pi E^* h_a) P_a$ for different values of $\alpha = (2\sqrt{2}/\pi)(\sqrt{L}/h_a)(W_{ad}/E^*)^{1/2}$. Note that c/L cannot exceed $1/2$ since the two surfaces are “flattened” when $c = L/2$. For $\alpha < 3^{3/4}/4 \approx 0.57$, maximum tensile and compressive force occurs at η_1 and η_2 , respectively. When $\alpha = 3^{3/4}/4$, $\bar{P}_a > 0$ for all c/L so that the surfaces will heal spontaneously without applied load.

contact in a load-controlled test until the normalized contact length reaches a value of $\eta_1 \approx (\alpha/4)^{2/3}/\pi$. The increase in contact length is stable after η_1 is reached; that is, to increase contact beyond η_1 , it is necessary to increase the compressive force. Eventually, at $\eta = \eta_2$, the maximum compression \bar{P}_a^{\max} is reached. For $\eta > \eta_2$, there is no equilibrium solution so that in a load-controlled test the surfaces will spontaneously heal. For $\alpha \leq 0.2$, $\eta_2 \approx 1/2 - \pi^{-1}(\alpha/4)^{2/5}$. The load required to achieve full contact can be found using (40a),

$$\bar{P}_a^{\max} = -\frac{\pi E^* h_a}{2} [\sin^2(\pi\eta_2) - \alpha\sqrt{\tan(\pi\eta_2)}] \approx -\frac{\pi E^* h_a}{2} (1 - 4^{1/5} \alpha^{4/5}) \quad (42)$$

From (42), it is clear that an upper bound for the load per asperity needed to achieve full contact is $\pi E^* h_a/2$. Thus, the minimum compressive stress σ_∞^c on the stamp for full contact is

$$\sigma_\infty^c = \frac{-a\pi E^* h_a}{2L(a+w)} \quad (43a)$$

The condition of full contact (43a) can be expressed in terms of a dimensionless parameter $\kappa_4 \equiv -\pi E^* h_a/(2\sigma_\infty L)$ as

$$\kappa_4 \equiv -\frac{\pi E^* h_a}{2\sigma_\infty L} \leq 1 + (w/a) \quad (43b)$$

Note the similarity between the condition for intimate contact (43b) and that for avoidance of roof collapse (13a). Indeed, by eliminating σ_∞/E between the two, one arrives at a necessary condition for microcontact printing that depends on geometrical parameters alone:

$$\frac{h}{w} \frac{\pi}{4(1+a/w)} \frac{1}{\cosh^{-1}[(\cos(w\pi/2(w+a)))^{-1}]} > \frac{\pi h_a}{2L(1+w/a)} \quad (43c)$$

In the limit of small w/a , this reduces to

$$\pi \frac{h_a}{L} < \frac{h}{w} \quad (43d)$$

Equations 43c,d quantify the necessary condition that for any material to simultaneously stamp out roughness without roof collapse, the aspect ratio of the roughness must be smaller than that of the roof cavity.

8. Stamp with Curved Reliefs

μ CP is carried out with stamps that have flat punches. With this geometry, the only way to reduce line width (contact length) is to decrease the punch width $2a$. One way of bypassing this limitation is to use punches with smooth curved profiles as shown in Figure 12, where the role of the asperities is now replaced by the punches on a stamp. Such geometry has several advantages. First, line width $2c$ can be regulated by varying the applied pressure σ_∞ on the stamp. Second, lateral instability and buckling are less likely since these punches have much greater bending stiffness.

As an example, consider the special case where the punch profile is described by (37), where h_a is now the punch height h and L is the spacing between punches.

The line width or contact length, $2c$, is given by (40a), where \bar{P}_a is to be interpreted as the load on each punch (P in previous sections). The only modification of the results in the last section is that (38) is replaced by

$$\sigma_\infty = P_a N = P_a/L \quad (44)$$

where $N = 1/L$ is the number of punches per unit length. Equations 44 and 37 completely determine the line width for a given stamp pressure provided that the work of adhesion between the elastomer and substrate is known. The work of adhesion can be measured using the JKR experimental technique.^{24–26} An advantage of this technique over other techniques (such as a peel test, for example) is its similarity to the stamping process.

There are limitations associated with curved punches. The minimum line width is dictated by η_1 , that is,

$$2c_{\min} \approx 2L(\alpha/4)^{2/3}/\pi = 1.7205 \left(\frac{L^2}{h_a} \sqrt{\frac{W_{ad}}{E^*}} \right)^{2/3} \quad (45)$$

For $L = 1 \mu\text{m}$, $h_a = \sqrt{5} \mu\text{m}$, $E^* = 1 \text{ MPa}$, and $W_{ad} = 50 \text{ mJ/m}^2$, the minimum line width is 0.37 microns.

9. Pull-Off Force

The force needed to separate a stamp from the substrate can be estimated using a fracture mechanics approach. Imagine small flaws of length Δa at the contact edges, as shown in Figure 14. The spaces between the punches can be viewed as the interior of internal cracks, each with length $2w$. This assumption is valid when $h/w \ll 1$. However, if this condition is not satisfied, then the solution

(24) Maugis, D.; Barquins, M. *J. Phys. D: Appl. Phys.* **1978**, *11*, 1989.

(25) Deruelle, M.; Leger, L.; Tirrell, M. *Macromolecules* **1995**, *28*, 7419.

(26) Chaudhury, M. K.; Weaver, T.; Hui, C. Y.; Kramer, E. J. *J. Appl. Phys.* **1996**, *80*, 30.

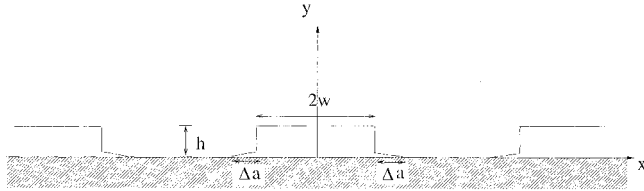


Figure 14. Schematic figure showing that the pull-off problem can be viewed as the failure of a periodic array of cracks of length $2(w + \Delta a)$ on the substrate/stamp interface, with a center to center distance of $2(w + a)$ and subjected to a uniform remote stress σ_∞ .

below (i.e., (48)) provides an upper bound for the pull-off stress. Thus, the pull-off problem can be treated as the failure of a periodic array of cracks of length $2(w + \Delta a)$ on the substrate/stamp interface, with a center to center distance of $2(w + a)$ as shown in Figure 14 and subjected to a uniform remote stress σ_∞ which is related to the stamp displacement Δ by (4). The stress intensity factors at the crack tips are identical and are given by Koiter¹²

$$K_I = \sigma_\infty [\pi(w + \Delta a)]^{1/2} [\xi^{-1} \tan \xi]^{1/2} \quad (46)$$

where

$$\xi = \pi(w + \Delta a)/[2(a + w)] \quad (47)$$

The condition for crack growth is $K_I = (2E^* W_{ad})^{1/2}$. This growth condition is based on the fact that the amount of elastic strain energy release per unit crack extension (energy release rate) is given by $K_I^2/2E^*$, where the factor of $1/2$ accounts for the rigid substrate. In equilibrium, the energy release rate must equal the work of adhesion. Equation 46 implies that K_I is an increasing function of Δa , and this means that crack growth is unstable so that the condition for pull-off is $K_I = (2E^* W_{ad})^{1/2}$. This allows us to compute the critical pull-off stress,

$$\sigma_\infty^{\text{pull-off}} = \sqrt{2E^* W_{ad}} (\pi w)^{-1/2} [\xi^{-1} \tan \xi]^{-1/2} \quad (48)$$

where Δa is assumed to be zero. According to (48), the pull-off stress increases with the elastomer modulus and the work of adhesion. Thus, increasing the modulus has a detrimental effect on the resolution and reliability of the punch. This is because a higher stress is needed to remove a stiffer stamp from a mold and this could cause local failure of the punches leading to lower resolution (e.g., fracture may not be along the elastomer/silicon interface). Equation 48 implies that the maximum pull-off force is reached in the limit $w/a \rightarrow 0$,

$$\sigma_\infty^{\text{pull-off}} = \sqrt{2E^* W_{ad}} (\pi w)^{-1/2} \quad (49)$$

In addition, it can be easily verified that $(\xi^{-1} \tan \xi)^{-1/2}$ is a monotonic decreasing function of w/a . Thus, decreasing the spacing between punches without increasing their width increases the pull-off force. Also, increasing the punch width $2a$ without changing the spacing increases the pull-off stress. In the limit of large w/a (very few punches), $\xi \rightarrow \pi/2$ and the pull-off stress goes to zero as expected. The dependence of the normalized pull-off stress $\bar{\sigma}_\infty^{\text{pull-off}}$ on w/a is shown in Figure 15. Note that the pull-off stress is normalized by its maximum $(2E^* W_{ad})^{1/2} (\pi w)^{-1/2}$, that is,

$$\bar{\sigma}_\infty^{\text{pull-off}} = \sigma_\infty^{\text{pull-off}} (\pi w)^{1/2} / \sqrt{2E^* W_{ad}} = (\xi^{-1} \tan \xi)^{-1/2} \quad (50)$$

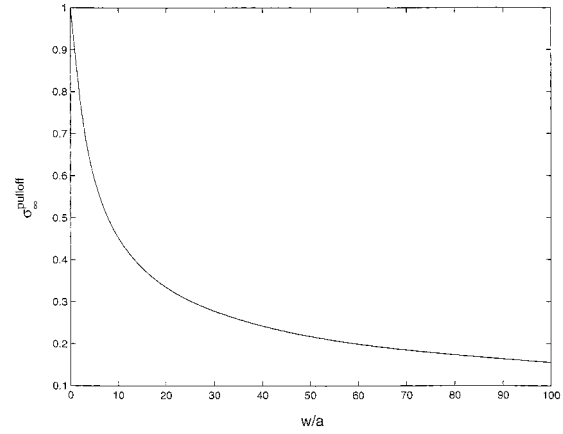


Figure 15. Dependence of the normalized pull-off force $\bar{\sigma}_\infty^{\text{pull-off}} = \sigma_\infty^{\text{pull-off}} (\pi w)^{1/2} / (2E^* W_{ad})^{1/2}$ on w/a .

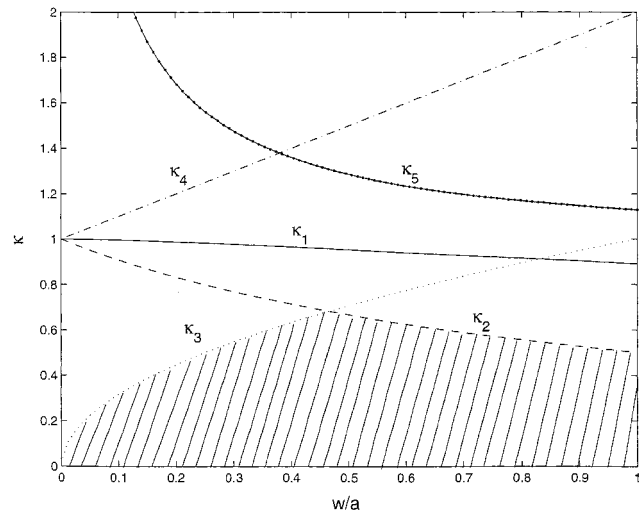


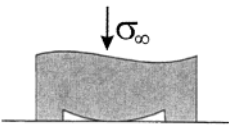
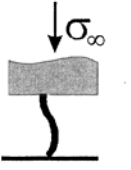
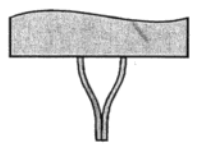
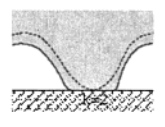
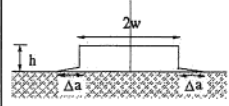
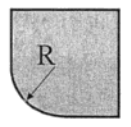
Figure 16. Stability and contact map. The horizontal axis is w/a . The vertical axis represents $\kappa_1, \kappa_2, \kappa_3, \kappa_4$, and κ_5 . The lines labeled are defined by (13a), (15b), (19b), (43b), and (51), respectively. Stability is assured if κ_1, κ_2 , and κ_3 lie below curves 1, 2, and 3. Good contact is assured if κ_4 lies below curve 4. Finally, pull-off is possible provided that the parameter κ_5 lies below curve 5. Thus, $\kappa_1, \kappa_2, \kappa_3, \kappa_4$, and κ_5 must all lie in the shaded region in Figure 12 to ensure dimensional stability, conformality, and pull-off.

An estimate of this maximum using $w = 1 \mu\text{m}$, $E^* = 1 \text{ MPa}$ and $W_{ad} = 50 \text{ mJ/m}^2$ is 0.18 MPa, or about $1/5$ of the elastic modulus. Thus, to achieve pull-off, the stamp must be pulled with a tensile stress exceeding $\sigma_\infty^{\text{pull-off}}$. This condition can be expressed in terms of a dimensionless parameter

$$\kappa_5 \equiv \sqrt{2E^* W_{ad}} / [\sigma_\infty^{\text{pull-off}} (\pi w)^{1/2}] \leq \sqrt{\frac{2(1 + w/a)}{\pi} \tan\left(\frac{\pi}{2(1 + w/a)}\right)} \quad (51)$$

A related issue is the maximum stress induced in the stamp during its release from the mold. The PDMS stamp is typically separated from the master by levering with an inserted wedge.⁶ The space between the inserted wedge and the punch closest to the wedge which is still in contact with the master can be viewed as an external crack. The minimum energy release rate needed to separate this punch from the master is W_{ad} . Thus, the minimum stress intensity factor is $(2E^* W_{ad})^{1/2}$. If we assume that the maximum normal stress σ_{max} occurs at a distance of a

Table 1. Summary of Results

| Description | Sketch (see also Fig. 1) | Result |
|---|---|--|
| 1. Roof collapse: unwanted contact |  | $\frac{4\sigma_{\infty} w}{\pi E^* h} \left(1 + \frac{a}{w}\right) \cosh^{-1} \left[\left(\cos \left(\frac{w\pi}{2(w+a)} \right) \right)^{-1} \right] < 1$ (13b) |
| 2. Buckling |  | $-\frac{1.47 \sigma_{\infty} h^2}{\pi^2 E^* a^2} < \frac{1}{1 + (w/a)}$ (15a) |
| 3. Lateral collapse |  | $\frac{h}{2a} \left(\frac{2\gamma_s}{3E^* a} \right)^{1/4} < \sqrt{w/a}$ (19b) |
| 4. Smooth surface asperities |  | $\frac{-\pi E^* h_a}{2\sigma_{\infty} L} < 1 + w/a$ (43b) |
| 5. Pull-off |  | $\frac{\sqrt{2E^* W_{ad}}}{\sigma_{\infty} (\pi w)^{1/2}} < \sqrt{\frac{2(1 + 2/a)}{\pi} \tan \left(\frac{\pi}{2(1 + w/a)} \right)}$ (51) |
| 6. Radius of an edge rounded by surface tension |  | $R \sim \frac{\gamma}{2E}$ Section 4 |

from the crack tip, then σ_{\max} is approximately given by $\sigma_{\max} = [2E^* W_{ad}/(\pi a)]^{1/2}$ which is on the same order as the pull-off stress.

Finally, eqs 46–51 have been derived assuming that a sharp crack nucleates prior to unstable separation of a stamp. It is possible that stamp separation is controlled rather by initiation of a crack at the interface, which would be governed by a cohesive separation stress condition.

10. Discussion and Summary

We have considered several modes of elastic deformation that may constrain the design of stamps for microcontact printing. Dimensional stability, conformality, and pull-off force are controlled by a set of dimensional parameters, κ_1 , κ_2 , κ_3 , κ_4 , κ_5 , and w/a (see (13b), (15b), (19b), (43b), and (51) for the definition of these parameters). These relationships, (13a), (15b), (19b), (43b), and (51), are summarized by a two-dimensional stability and contact map as shown in Figure 16 and in Table 1. The horizontal axis is w/a , accounting for that fact that κ_1 , κ_2 , κ_3 , κ_4 , and κ_5 depend only on w/a . The vertical axis represents κ_1 , κ_2 , κ_3 , κ_4 , and κ_5 . The five lines on Figure 16 are the curves

$$\frac{2\kappa_1}{\pi} \left(1 + \frac{a}{w}\right) \cosh^{-1} \left[\left(\cos \left(\frac{w\pi}{2(w+a)} \right) \right)^{-1} \right] = 1$$

(roof "collapse") (13a)

$$\kappa_2 = \frac{1}{1 + (w/a)} \quad (\text{buckling}) \quad (15b)$$

$$\kappa_3 = \sqrt{w/a} \quad (\text{lateral collapse}) \quad (19b)$$

$$\kappa_4 = 1 + (w/a) \quad (\text{stamp roughness}) \quad (43b)$$

and

$$\kappa_5 = \sqrt{\frac{2(1 + w/a)}{\pi} \tan \left(\frac{\pi}{2(1 + w/a)} \right)} \quad (\text{pull-off force}) \quad (51)$$

respectively. Stability requires that κ_1 , κ_2 , and κ_3 lie below curves 1, 2, and 3. Good contact is assured if κ_4 lies below curve 4. Finally, pull-off is possible provided that the parameter κ_5 lies below curve 5. Thus, κ_1 , κ_2 , κ_3 , κ_4 , and

κ_5 must all lie in the shaded region in Figure 16 to ensure dimensional stability, conformality, and pull-off.

We showed that surface tension will deform a sharp corner into a smooth shape with a radius of curvature on the order of γ_s/E . The internal stresses generated by surface tension in the vicinity of the corner can be very large. Closed form expressions for these stresses are presented.

Explicit expressions for the internal stresses in a stamp reinforced by a backplane have been given in closed form. We showed that the stress in the elastomer layer is typically on the order of $-E\Delta\epsilon_T$, where $\Delta\epsilon_T$ is the transformation strain due to chemical and thermal shrinkage.

Detailed calculations of contact pressure for various stamp geometries are also carried out both by analytical and by finite element methods. If the elastomer has smooth surfaces, then adhesive force alone is sufficient to bring the punches into intimate contact with the substrate.

Acknowledgment. C.Y.H. acknowledges a gift from the DuPont Company. E.J.K. acknowledges support from the National Science Foundation, Division of Materials Research, Polymers Program (Grant No.DMR-9803738), and the Materials Research Laboratory of UCSB (which is funded by the NSF-DMR-MRSEC Program).

LA0113567